Human Telomere Repeat Binding Factor TRF1 Replaces TRF2 Bound to Shelterin Core Hub TIN2 when TPP1 Is Absent

Tomáš Janovič, Martin Stojaspal, Pavel Veverka, Denisa Horáková and Ctirad Hofr

LifeB, Chromatin Molecular Complexes, CEITEC and Functional Genomics and Proteomics, National Centre for Biomolecular Research, Faculty of Science, Masaryk University, Brno CZ-62500, Czech Republic

Correspondence to Ctirad Hofr: hofr@sci.muni.cz
https://doi.org/10.1016/j.jmb.2019.05.038
Edited by Titia Sixma

Abstract

Human telomeric repeat binding factors TRF1 and TRF2 along with TIN2 form the core of the shelterin complex that protects chromosome ends against unwanted end-joining and DNA repair. We applied a single-molecule approach to assess TRF1–TIN2–TRF2 complex formation in solution at physiological conditions. Fluorescence cross-correlation spectroscopy was used to describe the complex assembly by analyzing how coincident fluctuations of differently labeled TRF1 and TRF2 correlate when they move together through the confocal volume of the microscope. We observed, at the single-molecule level, that TRF1 effectively substitutes TRF2 on TIN2. We assessed also the effect of another telomeric factor TPP1 that recruits telomerase to telomeres. We found that TPP1 upon binding to TIN2 induces changes that expand TIN2 binding capacity, such that TIN2 can accommodate both TRF1 and TRF2 simultaneously. We suggest a molecular model that explains why TPP1 is essential for the stable formation of TRF1–TIN2–TRF2 core complex.

Introduction

Human telomeres are maintained by telomerase [1,2] and protected by telomeric proteins [3,4]. Telomeric proteins recruit telomerase to telomeric DNA [5]. Shelterin is a six-protein complex comprising TRF1, TRF2, TIN2, TPP1, POT1 and RAP1. Shelterin associates specifically with telomeric DNA repeats and protects linear chromosome ends from being recognized by the DNA repair machinery as damaged DNA [4]. TRF1 and TRF2 (telomere repeat-binding factor 1 and 2) bind the double-stranded telomeric DNA [6,7]. TRF2 protects chromosomes by forming lasso-like structures through the invasion of the 3′ single-stranded overhang into the duplex telomeric repeats [8,9] while suppressing ATM activity [10]. RAP1 interacts solely with TRF2 and regulates the specific binding of TRF2 to telomeric DNA and subsequent telomeric loop processing by helicases [11,12]. TIN2 (TRF1-interacting nuclear factor 2) [13] binds both factors, TRF1 and TRF2 [4]. In addition, TIN2 recruits TPP1

("TPP1" combines the first letter of each name, TINT1 [14], PTOP [15] and PIP1 [16], from the three groups that initially characterized the human protein). TPP1 forms a heterodimer with POT1 (protection of telomeres 1) [17]. From the structural point of view, TIN2 is the central hub of the shelterin complex that links TRF1 and TRF2 homodimers with TPP1–POT1 heterodimers. The domains of TIN2 that take part in the interaction with TRF1, TRF2 and TPP1 are shown in Fig. 1a.

Regarding its biological functions, TIN2 is essential for telomere length regulation mediated by TRF1 [21,22]. TIN2 is required for TRF2-induced protection against ATM signaling pathway [23] and POT1-mediated protection against ATR signaling pathway [24,25]. In cells, TIN2 deletion compromises the stability of both TRF1 and TRF2 at telomeres [13,26]. TIN2 bridges TRF1 and TRF2 with TPP1, which then recruits telomerase to telomeres [5,27] and enhances telomerase processivity upon complexation with POT1 [28–30]. TIN2 is expressed in two isoforms with different biochemical and
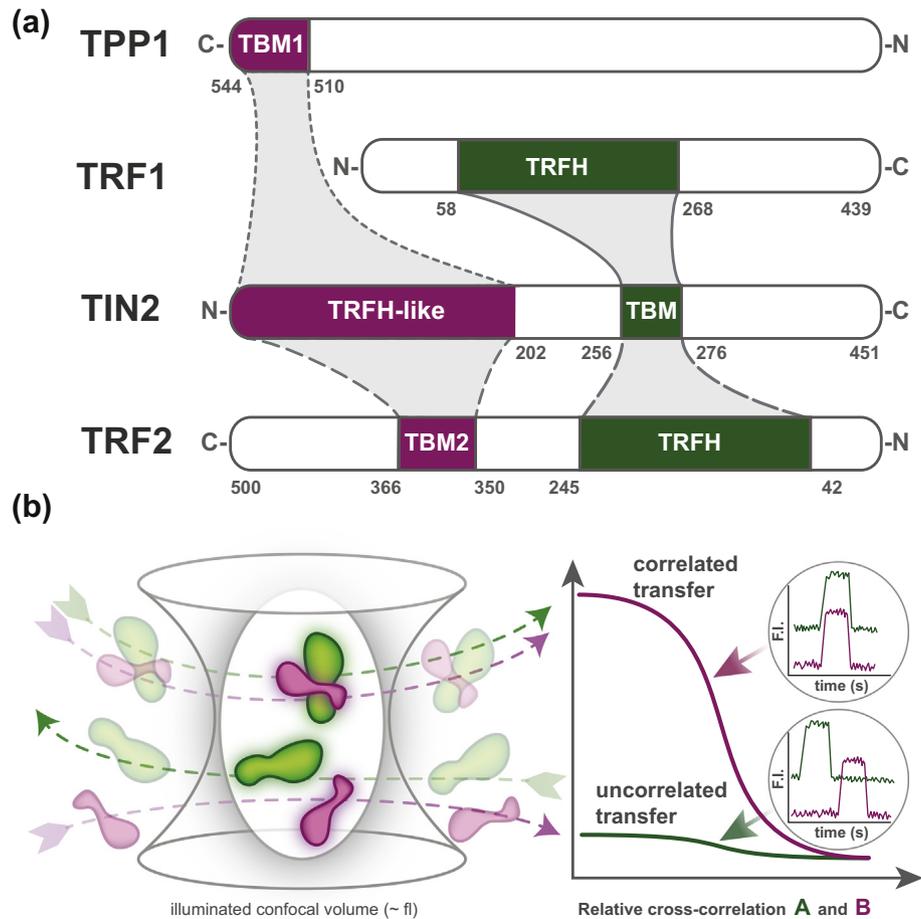
(a)

(b)

Fig. 1. TIN2 mediates the assembly of shelterin core proteins—interaction domains interconnect TIN2 with TRF1, TRF2 and TPP1. (a) Scheme of the studied proteins showing the interaction domains: TBM1, TIN2-binding motif of TPP1; TRFH, dimerization domain of TRF1 and TRF2; TRFH-like, dimerization domain of TIN2; TBM, TRFH of TRF1/TRF2 binding motif of TIN2; TBM2, TIN2-binding motif of TRF2. The more solid the outline stroke between the interacting domains, the higher their mutual affinity [18,19]. All identified interacting domains of shelterin proteins have been recently reviewed in Ref. [20]. (b) Scheme of how FCCS detects mutually bound proteins. When a green fluorescently labeled protein A and a red fluorescently labeled protein B diffuse through the illuminated confocal volume, fluorescence signals fluctuations are recorded simultaneously. If A binds B, the proteins move together, so they produce fluorescence intensity fluctuations of similar patterns for both fluorescence labels and the cross-correlation amplitude increases accordingly.

functional patterns [31]. Mutations in the gene of TIN2 have been implicated in approximately 15% of all known cases of *dyskeratosis congenita*—a disease that results in defective telomere mainte- nance in early childhood [32,33]. The assembly of shelterin subunits around TIN2 is critical for the formation of structurally and biologically functional shelterin complexes. The overall shelterin protein ratios on telomeres are known from *in vivo* experi- ments [34]. Newly, the *in vitro* stoichiometry of an assembled core complex comprising TRF2, TIN2, TPP1 and POT1 was revealed to be 2:1:1:1, respectively [35].

Previous studies described the structure and binding affinity of peptides representing interaction regions that take part in TRF1 and TRF2 binding to TIN2 [18]. Very recently, the structure of the isolated interacting domains of TRF2, TIN2 and TPP1 has been determined [19].

Furthermore, Hu *et al.* [19] postulated how structural changes in the TRFH-like domain of TIN2 (2–202) upon association with TPP1 domain TBM1 (544–510) increase the binding affinity of the TBM2 domain of TRF2 to TIN2. In addition, Kim *et al.* used isothermal titration calorimetry to reveal that the complexation of full-length TIN2 with TPP1 fragment (486–544), containing TBM1 domain, promotes association of TRF2 fragment (382–424) and TIN2 [36].

Despite the newly revealed structural–function relationships within shelterin at the domain level, very little is known about how full-length TRF1, TRF2

and TIN2 affect each other and TPP1 during shelterin assembly. The quantitative studies of shelterin proteins moving freely in solution represent an experimental challenge connected with the comparable size of TRF1 and TRF2 that excludes using simple fluorescence polarization measurements. Single-molecule approaches are powerful tools of assessing the functional states of a molecular system as has been demonstrated by assessing DNA-repair complex assembly and dynamics [36,37] along with mechanistic insights into telomeric proteins and telomerase function [38]. Nevertheless, classical single-molecule total internal reflection fluorescence microscopy is often limited to the area near the surface, where studied molecules are attached. Instead, by means of confocal scanning microscopy, we can measure interactions of fluorescently labeled proteins moving freely in solution regardless of the distance from the surface.

In this study, we took advantage of fluorescence cross-correlation spectroscopy (FCCS)—a single-molecule method that is based on an evaluation of the interdependence of time-resolved fluctuations of two different fluorophores by confocal microscopy [39]. FCCS monitors simultaneous fluorescence signals of two differently labeled proteins that diffuse through the confocal volume of a microscope objective (Fig. 1b) [40,41]. In particular, FCCS has been extensively used to describe the assembly of oligomeric calcium/CaM-dependent kinase II and calmodulin by the Schwille laboratory [39].

We used FCCS to monitor protein interactions *in vitro* based on the change in relative cross-correlation of differently labeled TIN2, TRF1 and TRF2 and to address the following hypotheses. First, we wanted to know whether both TRF1 and TRF2 bind TIN2 simultaneously or if there is an order preference during the shelterin subcomplex assembly. In addition, we tested the hypothesis that TPP1 binding to TIN2 may improve TRF2–TIN2 interaction and could enable TIN2 to interact simultaneously with TRF1 and TRF2, as has been suggested by the Songyang laboratory [42]. Finally, we wondered if we could suggest an interaction model of TRF1, TRF2, TIN2 and TPP1 assembly and correlate the model with available structural data and biological functions of shelterin proteins.

We found that TRF1 induces TRF2 release from TIN2. We also described that TPP1, upon binding to TIN2, improves TIN2's binding capacity so the complex TIN2–TPP1 can accommodate both TRF1 and TRF2. We showed for the first time with full-length TRF1 at the single-molecule level that TPP1 is essential for the formation of the stable TRF1–TIN2–TPP1–TRF2 complex. We suggest a mechanism that explains the mutual exclusivity of TRF1–TIN2 and TRF2–TIN2 interactions along with the requirement of TPP1 for simultaneous binding of TRF1 and TRF2 to TIN2. This work is, to our knowledge, the first single-molecule study describing the assembly of full-length proteins TRF1, TRF2 and TIN2.

Results

TRF1 replaces TRF2 bound to TIN2

At first, we wanted to know whether full-length TIN2 is able to accommodate both full-length TRF1 and TRF2 simultaneously. We allowed forming complexes of TRF1–TIN2 and TRF2–TIN2 at micromolar concentrations as suggested by dissociation constants obtained from our microscale thermophoresis assay (Supplementary Fig. S5). The complexes TRF1–TIN2 and TRF2–TIN2 were prepared with 2:1 stoichiometry. Subsequently, the complex solutions were diluted to the concentration required for a single-molecule detection. For our FCCS measurements, TRF1 or TRF2 (20 nM) was labeled with red fluorophore Alexa Fluor 594 and TIN2 (10 nM) was labeled with the green fluorophore Alexa Fluor 488.

In the first experiment, we titrated dual-labeled TRF2–TIN2 complex with unlabeled TRF1 to a final concentration of 80 nM (Fig. 2a and b). Initially, when the TRF2–TIN2 mixture was measured, we observed a high relative cross-correlation corresponding to the relative cross-correlation of the positive control (Supplementary Fig. S1). Thus, we can affirm that the TRF2–TIN2 complex was stably formed. Immediately after the addition of 2.5 nM of TRF1, we observed that the relative cross-correlation between TIN2 and TRF2 decreased to the level of the negative control (Supplementary Figs. S1 and S2). Overall, the decrease of relative cross-correlation suggested that TRF1 replaced TRF2 in the complex with TIN2 (Fig. 2a and b).

TRF2 showed no influence on TRF1–TIN2 complex

In the next sets of experiments, we used a reverse arrangement where TRF1 labeled with red fluorophore (Alexa Fluor 594) was allowed to bind TIN2 labeled with green fluorophore (Alexa Fluor 488). Subsequently, we added unlabeled TRF2 gradually and monitored if TRF2 can disturb the complex TRF1–TIN2. We measured the relative cross-correlation of labeled TRF1 and TIN2 at each concentration of unlabeled TRF2 (Fig. 2c and d). The relative cross-correlation of TRF1 and TIN2 remained high and stable at TRF2 concentration up to 80 nM. In other words, when we added TRF2 to the preformed complex TRF1–TIN2, we detected no significant decrease of relative cross-correlation between TRF1 and TIN2 (Supplementary Fig. S2). The minimal effect of TRF2 presence on TRF1–TIN2 relative cross-correlation suggested that TRF2 did not disturb the TRF1–TIN2 complex.

TRF2 has no effect on DNA binding affinity of TRF1–TIN2

We also wanted to assess whether the presence of TRF2 affects the binding of TRF1 to telomeric
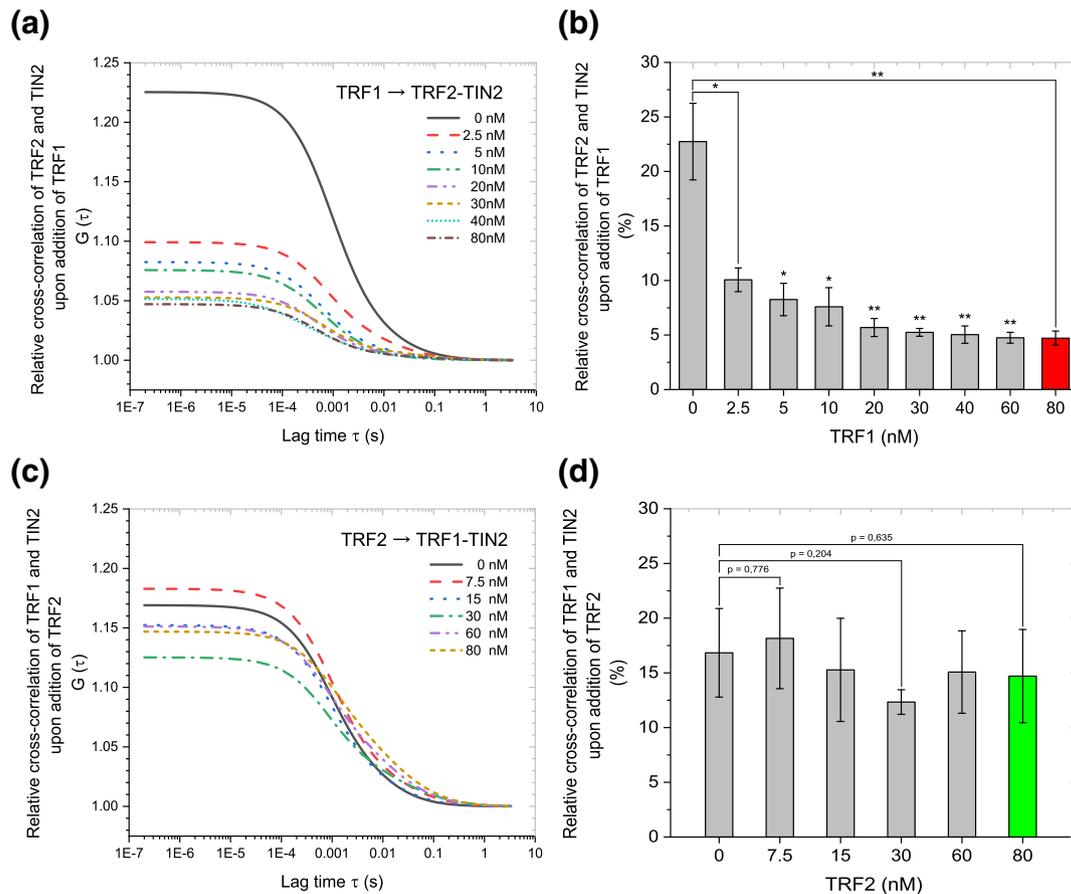
Fig. 2. TRF1 replaces TRF2 from TIN2, whereas TRF2 has no effect on TRF1–TIN2 complex. (a) The relative cross-correlation of fluorescently labeled TRF2 (20 nM) and TIN2 (10 nM) measured upon addition of unlabeled TRF1 (0–80 nM). Fits of relative cross-correlation curves upon increase of TRF1 show a decrease of the amplitude of TRF2–TIN2 relative cross-correlation. (b) The amplitudes of TRF2–TIN2 relative cross-correlation at 0–80 nM TRF1 presence—determined from panel a. Error bars represent standard deviations of three independent measurements. *P*-values: two-tailed Student's *t* test with regard to the amplitude without TRF1 (0 nM); *$P < 0.05$, **$P < 0.01$. (c) The relative cross-correlation of fluorescently labeled TRF1 (20 nM) and TIN2 (10 nM) measured upon addition of unlabeled TRF2 (0–80 nM). Fits of relative cross-correlation curves upon increase of TRF2 show that the amplitude of TRF2–TIN2 relative cross-correlation stays at the initial level. (d) The amplitudes of TRF1–TIN2 relative cross-correlation at 0–80 nM TRF2 presence—determined from panel c. Error bars represent standard deviations of three independent measurements. *P*-values: two-tailed Student's *t* test with regard to the amplitude without TRF2 (0 nM).

DNA when TRF1 is in complex with TIN2. To analyze how mutual TRF1, TRF2 and TIN2 interactions affect DNA binding affinity, we employed fluorescence anisotropy (Fig. 3). For this purpose, we used a telomeric DNA duplex R5 containing five telomeric repeats and a stoichiometric combination of TRF1, TRF2 and TIN2, 2:2:1, respectively, as has been suggested previously [34,35]. R5 should feasibly accommodate both TRF1 and TRF2 simultaneously. Our quantitative binding data revealed that the DNA binding affinity of the stoichiometric combination of TRF1, TRF2 and TIN2 is similar to the DNA binding affinity of the combination TRF1 and TIN2. In other words, TRF2 did not affect the DNA binding affinity of TRF1–TIN2.

TPP1 enables TIN2 to accommodate both TRF2 and TRF1 simultaneously

We wondered whether another human telomeric protein TPP1 improves the stability of TRF1–TIN2–TRF2 complex consisting of full-length proteins. Hu *et al.* suggested that the C-terminal domain of TPP1 is responsible for its binding to TIN2 and that TPP1 stabilizes the TIN2–TRF2 interaction [19]. The full-length TPP1 purity was insufficient for single-molecule experiments; thus, recombinant human TPP1 with an N-terminal deletion was used. TPP1 (89–554) was chosen because the 88 N-terminal residues of TPP1 are functionally dispensable in human cells and are not conserved among TPP1
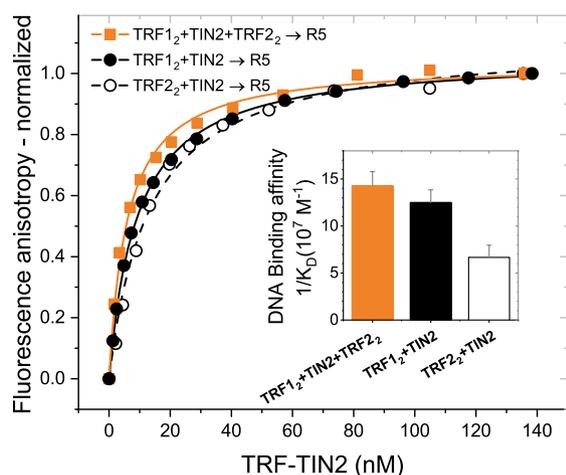
Fig. 3. DNA binding affinity of stoichiometric combination of TRF1/TIN2/TRF2 (2:1:2) is similar to DNA binding affinity of stoichiometric combination of TRF1/TIN2 (2:1). TRF1 (5 μM) and/or TRF2 (5 μM) was incubated with TIN2 (2.5 μM) in 50 mM sodium phosphate (pH 7.0) and 50 mM NaCl at 25 °C. Protein solutions were titrated to Alexa Fluor 488-labeled telomeric DNA duplex R5 containing five telomeric repeats. The presented binding isotherms are averages of five independent experiments with standard deviation lower than 3% for each presented data point. The inset bar plot shows reciprocal K_D values that correspond to DNA binding affinity.

proteins of different organisms [16,30,43]. In addition, TPP1 (89–554) still contains the N-terminus of the OB domain that is critical for telomerase activity [44]. For simplicity, we hereafter use TPP1 to refer to TPP1 (89–554) unless stated otherwise.

We incubated fluorescently labeled TRF2 and TIN2 along with unlabeled TPP1 at room temperature. Then, we added unlabeled TRF1 to see whether TRF1 can still remove TRF2 from the TIN2–TPP1–TRF2 complex. As Fig. 4a shows, relative cross-correlation between TRF2 and TIN2 remained at high levels for all concentrations of TRF1. The relative cross-correlation between TRF2 and TIN2 was changed insignificantly according to calculated *P*-values (Fig. 4b). The statistically insignificant change of relative cross-correlation suggested that the majority of TRF2 remains bound to TIN2–TPP1 in the presence of TRF1.

The formation of the complex TRF1–TIN2–TPP1–TRF2 was confirmed by a complementary FCCS experiment where TRF1 and TRF2 were labeled by Alexa Fluor 488 and Alexa Fluor 594, respectively. First, unlabeled TIN2 was added to the mixture of labeled TRF1 and TRF2. After TIN2 addition, we observed no significant change in the amplitude of relative cross-correlation between TRF1 and TRF2 (Fig. 4c). On the contrary, when we added preformed

complex of TIN2–TPP1 into TRF1 and TRF2 mixture, we detected a substantial increase of relative cross-correlation between TRF1 and TRF2 (Fig. 4c).

When we mixed TRF1, TIN2, TRF2 and TPP1 together, we observed high relative cross-correlation between TRF1 and TRF2, similar to the relative cross-correlation between TRF2 and TIN2 in the previous experimental setup (compare Fig. 4a and c). The high relative cross-correlation level in both experimental arrangements verified that the TRF1–TIN2–TPP1–TRF2 complex was formed.

To confirm that the proteins form a stable complex, we recorded size-exclusion chromatography profiles of a mixture comprising TRF1, TIN2 and TRF2 with or without TPP1 (Fig. 4d). Only in the presence of TPP1 we observed a high-molecular peak that corresponds to the assembled protein complex (compare the solid red line and dashed blue line in Fig. 4d). We analyzed collected chromatographic fractions by SDS gel electrophoresis. As TRF1 and TRF2 were labeled by different fluorophores, we identified electrophoretic bands corresponding to TRF1 and TRF2 (insets in Fig. 4d). The fluorescence intensity profiles showed that TRF1 and TRF2 formed a complex only if TPP1 and TIN2 were present. Furthermore, the collected fractions were characterized by dynamic light scattering to verify that TRF1–TIN2–TRF2–TPP1 complex was formed (Fig. S9).

In addition, we have carried out control measurements with TIN2 mutants that were unable to bind TPP1 or TRF2. We have prepared two TIN2 point mutants—A15R and A110R. The A15R mutation inhibits TPP1 binding and the A110R mutation inhibits TRF2 binding to the N-terminus of TIN2, as revealed by Hu *et al.* [19]. Our FCCS measurements showed that both mutations of TIN2 restricted the assembly of the shelterin core complex (Supplementary Fig. S4). We found that TIN2 A110R was unable to form complex with TRF2 even in the presence of TPP1 and TRF1 (Supplementary Fig. S4a).

The inability of TIN2 A110R to bind TRF2 indicates that N-terminal binding site of TIN2 is critical for the stable accommodation of TRF2 into the complex. FCCS measurements with the second mutant revealed that TIN2 A15R, with impaired TPP1 binding ability, was unable to cross-correlate with TRF2 in the presence of TRF1 and TPP1 (Supplementary Fig. S4b). Thus, FCCS experiments with TIN2 mutants supported the view that the N-terminal domain of TIN2 is essential for the cooperative binding of TRF2 and TPP1 to TIN2. In summary, our combined single-molecule and ensemble analyses of shelterin core proteins suggest that TPP1 enables TIN2 to bind both TRF1 and TRF2 simultaneously and form stable TRF1–TIN2–TPP1–TRF2 complex.
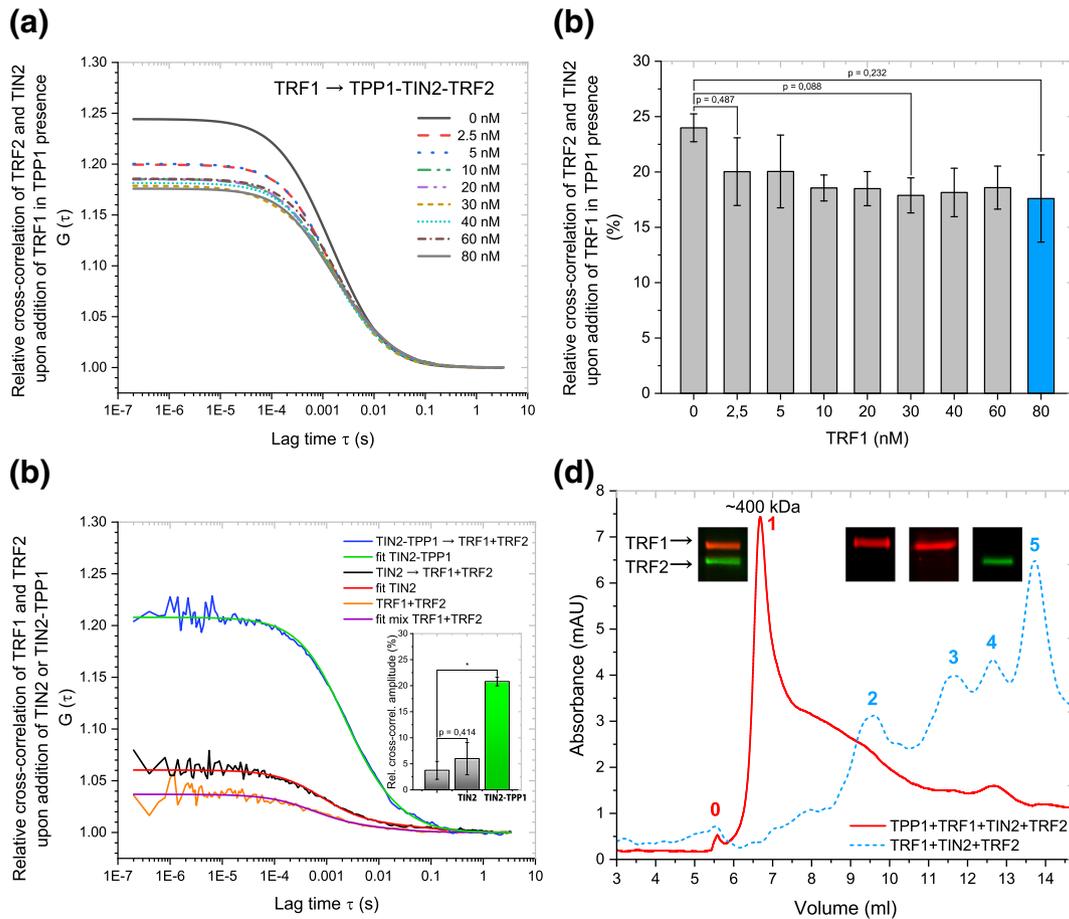
(a)

(b)

(b)

(d)

Fig. 4. TPP1 enhances the formation of TRF1–TIN2–TRF2 complex—TRF2 remains bound to TIN2–TPP1 complex in TRF1 presence. (a) Alexa Fluor 488-labeled TIN2 (10 nM) and Alexa Fluor 594-labeled TRF2 (20 nM) were incubated in stoichiometric ratio with unlabeled TPP1 (10 nM) at 25 °C. Fits of relative cross-correlation between TRF2 and TIN2 upon addition of unlabeled TRF1 to TRF2–TIN2–TPP1 complex show significant cross-correlation in TRF1 presence up to 80 nM. (b) The amplitudes of TRF2–TIN2 relative cross-correlation in TPP1 presence upon TRF1 addition—determined from panel a. Error bars represent standard deviations of three independent measurements. *P*-values: two-tailed Student's *t* test with regard to the amplitude without TRF1 (0 nM). (c) Relative cross-correlation of Alexa Fluor 594-labeled TRF1 (20 nM) and Alexa Fluor 488-labeled TRF2 (20 nM) measured upon addition of unlabeled TIN2 (10 nM) or preformed TIN2–TPP1 complex (10 nM). Upon addition of preformed TIN2–TPP1 complex, the significant increase of relative cross-correlation of TRF1 and TRF2 was observed. The TRF1–TIN2–TPP1–TRF2 complex was formed only if TPP1 was present. The inset bar plot shows the increase of TRF1–TRF2 relative cross-correlation upon addition of TIN2–TPP1 complex or TIN2 alone. *P*-values: two-tailed Student's *t* test with regard to the amplitude of TRF1 and TRF2 mixture only; *P < 0.05. (d) Size-exclusion chromatography traces of TRF1, TIN2, TPP1, TRF2 (solid line) and TRF1, TIN2, TRF2 (dashed line). TRF1 and TRF2 were labeled by Alexa Fluor 594 and Alexa Fluor 488, respectively. Fractions corresponding to the numbered peaks were collected and analyzed on SDS-PAGE. Peak 0 corresponds to the void fraction. Peak 1 contains both labeled proteins within TRF1–TIN2–TPP1–TRF2 complex. Peak 2 represents TRF1–TIN2; peak 3, TRF1; peak 4, TRF2; peak 5, TIN2. Dynamic light scattering measurements verified TRF1–TIN2–TPP1–TRF2 complex formation (Fig. S9).

Discussion

Our findings of how human telomeric proteins TRF1 and TPP1 affect the formation of the core shelterin complex TRF1–TIN2–TRF2 have provided new insights into the assembly of the full shelterin complex at the single-molecule level. In addition, our study has contributed to address the following biological questions about human shelterin:

(i) What are the arrangements of shelterin proteins TRF1, TRF2 and TIN2 in solution without DNA? (ii) How does the shelterin core TRF1–TIN2–TRF2 assemble? (iii) How can TPP1 affect TRF1–TIN2–TRF2 complex formation? We address these questions below.

Our quantitative biophysical observations clearly showed that TIN2 binds either TRF1 or TRF2. Thus, two independent complexes TRF1–TIN2 and TRF2–

TIN2 appear in solution. The observation of mutual exclusive binding of TRF1 or TRF2 to TIN2 is in agreement with previous studies. O'Connor *et al.* [42] have suggested that TRF1–TIN2 and TRF2–TIN2 occur as separate sub-complexes based on immunoprecipitation studies. In addition, when we take into consideration available information about the positions of interacting domains, domain structure and quantitative binding characterizations, we can rationalize why TRF1 replaces TRF2 on TIN2. So far, it seemed that the shelterin proteins form hetero-multimeric complexes through a selective domain-domain interaction mechanism.

As Chen *et al.* [18] showed, both TRF2 and TRF1 can bind one common binding site TBM (TRFH-binding motif Fig. 1a) on TIN2. TBM at the C-terminus of TIN2 is a well-structured 256–276 region that interacts with TRFH domain of both TRF1 and TRF2. The surface of TBM matches better the hydrophobic interface of TRFH domain of TRF1 than the polar interface of TRFH domain of TRF2. The different structural arrangements of interaction interfaces prompt the TRFH domain of TRF1 to bind a peptide representing the TBM region of TIN2 with higher binding affinity than the TRFH domain of TRF2 [18].

In addition, there is another well-structured binding site at TIN2's N-terminus (TRFH-like) where TRF2 binds with higher affinity compared to the previously mentioned common TRF1/TRF2 binding site TBM. If we consider that interactions between proteins occur mainly through the minimal identified domains, we may expect similar binding affinity for full-length proteins. Thus, TRF1 may form a complex with TIN2 more readily than TRF2. The higher binding affinity of TRF1 to TIN2 causes higher preference for the formation of the complex TRF1–TIN2 compared to TRF2–TIN2.

We determined the ensemble binding affinity of full-length TRF1 to TIN2 and TRF2 to TIN2 by microscale thermophoresis (Supplementary Fig. S5). Here, the obtained binding affinities for full-length proteins are higher than the affinities for isolated domains measured by Chen *et al.* [18] and Hu *et al.* [19]. The elevated binding affinity might suggest that additional hydrophobic and hydration effects promote full-length protein interactions [45].

If we consider the higher binding affinity of TRF1 to TIN2, we suppose that the TRF1–TIN2 complex incidence should prevail over the TRF2–TIN2 complex occurrence. In addition, if there was no other binding site on TIN2 for TRF2 or a binding regulation mechanism, the probability of forming complex TRF1–TIN2–TRF2 would be significantly low. The second binding site for TRF2 on TIN2 (TRFH-like domain, Fig. 1a) should allow the formation of the tri-functional complex TRF1–TIN2–TRF2.

In this context, our finding that TRF1 can substitute TRF2 when bound to TIN2 was rather unexpected at first glance (Fig. 2a and b). However, we can rationalize the TRF2 displacement when we consider that TRF1 binding affinity to TIN2 is higher [19] than TRF2 binding to TBM on TIN2 [18], as supported by our microscale thermophoresis measurements with full-length proteins (Supplementary Fig. S5). Let us assume that TRF2 binds TRFH-like domain of TIN2 in TRF1 absence, as TRF2 should occupy the binding site with the highest affinity at first. When TRF1 appears in TIN2–TRF2 complex proximity, TRF1 binds TBM site on TIN2.

We observed that the relative cross-correlation between TRF2 and TIN2 decreased even before the equal concentration of TRF1 and TRF2 was reached (Fig. 2a). We may hypothesize that (i) TRF1 binding to TIN2 affects TRF2 release catalytically; (ii) TRF1 simultaneously binds several TRF2–TIN2 subunits; and (iii) TRF2 forms aggregated clusters that are released from TIN2 by TRF1 before the expected equimolar ratio TRF1:TRF2 is achieved. The last explanation seems to be the most probable regarding our observation that TRF2 aggregates on DNA (Fig. S6, Video 1). Unfortunately, based on the available data, we could not determine the main cause of the premature drop of relative cross-correlation.

Why is TRF2 released upon TRF1 binding when there are two independent binding sites for TRF1 and TRF2? One straightforward explanation would be that TRF1 bound to TIN2 presents a steric hindrance that disturbs the optimal interaction surface between TRF2 and TIN2. The second explanation could be that TRF1 induces structural changes in TRFH-like domain of TIN2 that disable TRF2 binding to TIN2. Moreover, there could be a combination of both—steric hindrance and structural changes. Nevertheless, TRF2 binding to TRF1–TIN2 must be promoted to form the stable core complex TRF1–TIN2–TRF2.

As the first, O'Connor *et al.* [42] suggested that TPP1 promotes the interaction between TIN2 and TRF2. Recently, Hu *et al.* have shown that the binding of TPP1 interacting domain to TIN2 allosterically changes the TRF2 binding site on TIN2 TRFH-like domain [19]. Furthermore, this study revealed that the binding affinity between minimal interaction domains of TPP1–TIN2 and TRF2 was increased almost 3-fold if compared to the interaction without TPP1 [19].

As TPP1 induces allosteric changes on TIN2 that open the second binding site and thus increase TRF2 binding affinity, TPP1 promotes the stable formation of TRF1–TIN2–TPP1–TRF2 complex. Our single-molecule FCCS results support the view that TPP1 acts as a shelterin assembly activator. We corroborated that TRF2 remained bound to TIN2 in TRF1 presence and TRF1–TIN2–TRF2 complex was formed when TPP1 was bound to TIN2 (Fig. 4a and c). We summarize our recent results within the framework of the present state of knowledge of shelterin core assembly in the model below.
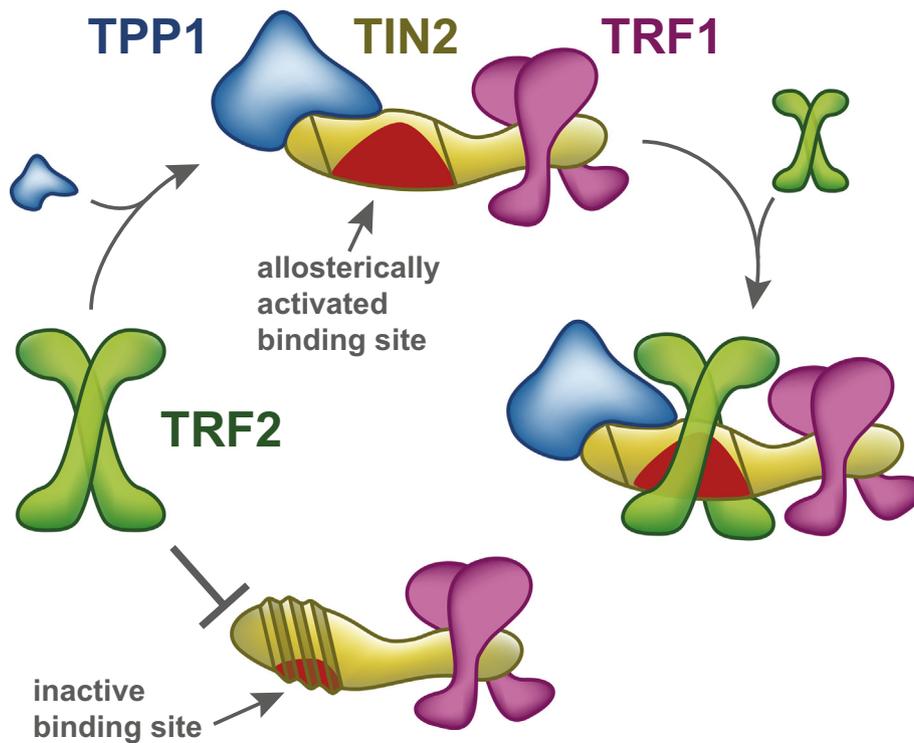
Fig. 5. A model for sequential assembly of shelterin core complex TRF1–TIN2–TRF2. TRF1 prevents TRF2 from binding to TIN2 if TPP1 is absent, as TRF1 occupies the preferential binding site on TIN2 (lower part of the scheme). On the contrary, when TPP1 binds TIN2, TPP1 induces structural changes that open the second binding site on TIN2, and the binding site for TRF2 becomes active (upper part of the scheme). TRF2 binds TIN2–TPP1 along with TRF1 (middle part of the scheme). A stable shelterin core complex TRF1–TIN2–TPP1–TRF2 is formed.

Model of core shelterin assembly

We propose a model of how shelterin core proteins assemble in solution. The model takes into consideration that TRF1 and TRF2 form homodimers [46,47], as the homodimerization exclusivity of TRF1 and TRF2 is a functional requirement that facilitates separation of different functions for both TRF proteins of similar domain structures. The model also reflects the stoichiometry of shelterin proteins that has been revealed by the de Lange and the Cech laboratories [34,35].

The recommended model suggests that if TRF1 occupies the TBM binding site on TIN2, TRF2 binding to TIN2 is compromised—only TRF1 remains bound to TIN2 (Fig. 5). When TPP1 binds TIN2, the N-terminal binding site of TIN2 becomes active. Subsequently, TRF2 can bind TIN2 also in TRF1 presence. Thus, TPP1 activates the N-terminal binding site for TRF2 on TIN2 and enables TIN2 to accommodate both TRF1 and TRF2 simultaneously. The model suggests that the protein order during shelterin core self-assembly in solution is TRF1 > TIN2 > TPP1 > TRF2.

In addition, the model explains the unique ability of TRF1 to exclude TRF2 from the complex TRF2–TIN2. Our model suggests that TRF1–TIN2 is an initial complex based on the highest affinity between TIN2 and TRF1 among shelterin proteins [18]. Moreover, TRF1–TIN2 preferential binding explains why it is not possible to prepare TRF1–TIN2–TRF2 complex without TPP1. The model is in agreement with recent findings that suggest that TPP1 induces allosteric structural changes on TIN2 to open the N-terminal TRF2 binding site [19]. As Hu *et al.* showed by fluorescence polarization measurements, TPP1 upon binding to TIN2 increases the affinity of the interacting domains of TRF2 to TIN2 [19]. Accordingly, Kim *et al.* [48] used isothermal titration calorimetry to detect 17-fold increase in binding affinity of TRF2 and TIN2 upon complexation with TPP1. Thus, the induced structural changes allow tighter binding of TRF2 to TIN2 without the compromising effect of the prebound TRF1.

The model with two TRF2 binding sites on TIN2 has been supported by our FCCS experiments with mutated variants of TIN2 (Supplementary Fig. S4). We observed no cross-correlation for TIN2 mutants that were unable to bind TPP1 or TRF2 on the N-terminus of TIN2. The point mutations of TIN2 prevented the complexation of TRF1 and TRF2. The model supports the view that the N-terminal

binding domain of TIN2 is essential for the cooperative binding of TRF2 and TPP1 to TIN2 and promoting assembly of TRF1–TIN2–TRF2–TPP1 complex.

In addition, we carried out FCCS experiments with monomeric TRF2V$_{52D,N53P}$—the construct with impaired self-dimerization [49]. We observed that the relative cross-correlation between fluorescently labeled TRF2V$_{52D,N53P}$ and fluorescently labeled TIN2 was diminished upon unlabeled TRF1 addition (Supplementary Fig. S10a and b). In other words, TRF1 released monomeric TRF2V$_{52D,N53P}$ from TIN2. Furthermore, we have carried out the control titration of TRF1 to TRF2V$_{52D,N53P}$–TIN2–TPP1 (Supplementary Fig. S10c and d). The comparison of the control titration with the experiment when TRF1 was titrated into TRF2V$_{52D,N53P}$–TIN2 (Supplementary Fig. S10a and b) shows that TRF1 releases TRF2 also when TRF2 is in the monomeric form. The lower deviation of relative cross-correlation amplitudes observed when TRF1 was titrated into monomeric mutant TRF2 containing complex TRF2V$_{52D,N53P}$–TIN2–TPP1 (Fig. S10c) compared to the deviation of relative cross-correlation amplitudes when TRF1 was titrated into wild-type TRF2–TIN2–TPP1 (Fig. 4a) might be because the monomeric TRF2V$_{52D,N53P}$ prevents nonspecific interactions with TIN2. We observed that TRF1 induced the release of monomeric TRF2V$_{52D,N53P}$ from TIN2 in similar extent as the release of wild-type TRF2 from TIN2 (Fig. 2a and b), which further supports the suggested binding mechanism. Thus, the proposed model is robust that it may be extended to TRF2 that binds to TIN2 as a monomer.

The proposed model is applicable also to mechanisms where proteins first form weak transient complexes, and then depend on the additive energies of binding and structural changes provided by partner proteins to generate higher specificity. Finally, it should be pointed out that the intrinsic dynamics of TRF1 and TRF2 could be important for regulating the assembly and disassembly of shelterin complexes, and exchanging between capped and uncapped telomere structures [50]. Based on here documented single-molecule studies, we suggest that TIN2–TPP1 binding could function as a switch to allow complete shelterin assembly containing TRF1 that associates with double-stranded DNA and TRF2 that associates mainly with the double-strand/single-strand junction of telomeric DNA. Thus, TPP1 binding seems to be critical for the whole shelterin assembly. Then the complete shelterin could accumulate on telomeres properly and maintain its regulatory functions regarding telomerase access and activity. Recently, we revealed that the interaction of TIN2 and TPP1 shows the lowest affinity within shelterin subunits *in vitro* [51]. Thus, TPP1–TIN2 interaction is a limiting step during shelterin reconstitution. Hence, our results

along with recent functional and structural studies advocate that TPP1–TIN2 interaction is crucial for both—functional shelterin assembly and dynamics of shelterin reconstitution.

In summary, our study with full-length human telomeric proteins TRF1, TRF2 and TIN2 brings new information about the assembly of shelterin subcomplexes. Our results with the core shelterin complex TRF1–TIN2–TRF2 extend the knowledge, so far limited to previous structural and functional studies of shelterin assembly that have been carried out without TRF1. For the first time, we applied single-molecule approaches to monitor TRF1, TRF2, TIN2 and TPP1 during their assembly in solution. The presented studies describe how the mutual arrangement of functional subcomplexes of telomeric proteins contribute to the role of the whole shelterin in telomere protection. The next challenging tasks will be to monitor the dynamics of the shelterin complex assembly in living cells.

Material and Methods

Cloning, expression and purification of TRF1, TRF2, TIN2 and TPP1

The cDNA sequences of TRF1, TRF2, TIN2 and TPP1 were synthesized by Source BioScience and cloned to pDONR/Zeo vector (Life Technologies) using two sets of primers and BP clonase enzyme mix from Gateway technology (Life Technologies). The resulting plasmids were cloned into different expression vectors in a recombination reaction using LR clonase enzyme mix (Life Technologies) and expressed as His-tagged proteins in different strains of *Escherichia coli* (pUbiKan_X105_TRF1 and pHGWA_TRF2 in BL21(DE3), pTriEx4_TIN2 in C41 and pRbXKan_x105_TPP1-FL (89–554) in BL21 (DE3) RIPL. BL21(DE3) and C41 cells harboring TRF1, TRF2 and TIN2 were grown in Luria-Bertani medium, and BL21(DE3) RIPL cells with TPP1 were grown in Terrific Broth medium, containing 50 µg ml^{-1} kanamycin (TRF1, TPP1) or 100 µg ml^{-1} ampicillin (TRF2, TIN2) or 34 µg ml^{-1} chloramphenicol (TPP1) at 37 °C until A_{600} reached 0.5 (TPP1) or 1.0 (TRF1, TRF2, TIN2). The cells were cultured for 3 h at 15 °C (TRF1, TPP1) or 25 °C (TRF2, TIN2) after the addition of IPTG to the final concentration of 0.5 mM (TRF1, TIN2, TPP1) or 1 mM (TRF2). Cells were collected by centrifugation (8000*g*, 8 min, 4 °C).

The pellet was dissolved in lysis buffer containing 50 mM sodium phosphate (pH 8.0), 500 mM NaCl, 10 mM imidazole (TRF1, TRF2, TIN2) or 20 mM imidazole (TPP1), 0.5% Tween-20 (TRF1, TRF2, TIN2) or 0.5% Triton X-100 (TPP1), 10% glycerol, and protease inhibitor cocktail cOmplete tablets EDTA-free (Roche). The cell suspension was

sonicated for 3 min of process time with 1-s pulse and 2 s of cooling on ice (Misonix). Cell lysate supernatant was collected after centrifugation at 20,000g, 4 °C for 1 h. Proteins were purified by immobilized-metal affinity chromatography using TALON® metal affinity resin (Clontech), where filtered supernatant (0.45 μm filter) was mixed with TALON® beads and incubated for 30 min. The proteins of our interest were eluted at 200 mM (TIN2), 300 mM (TPP1) or 500 mM (TRF1, TRF2) imidazole in the same buffer without Tween-20 or Triton X-100. TRF2 and TIN2 were dialyzed into 50 mM sodium phosphate (pH 7.0) and 50 mM NaCl. TRF1 was loaded onto the HiLoad 16/600 column containing Superdex 200 pg (GE Healthcare Life Sciences) and resolved using 50 mM sodium phosphate buffer (pH 7.0) with 200 mM NaCl. TRF1 was expressed and purified with tags His, S and Ubi to extend the protein stability during FCCS experiments at 25 °C. Tags on TRF1 did not affect FCCS measurements, as documented in Supplementary Fig. S11. TPP1 expression tags were removed by HRV3-C protease at 4 °C for 2 h with 3 mM DTT. The final purification was on HiLoad Superdex 200 pg column (GE Healthcare Life Sciences) equilibrated with buffer containing 50 mM sodium phosphate (pH 7.0) and 800 mM NaCl. The proteins were concentrated and the buffer was exchanged to 50 mM sodium phosphate (pH 7.0), 50 mM NaCl (TRF1, TRF2, TIN2) or 150 mM NaCl (TPP1) by ultrafiltration (Amicon 3 K/30 K, Millipore).

The concentration of purified proteins was determined by the Bradford assay. We evaluated protein purity by SDS-polyacrylamide gels stained by Bio-Safe Coomassie G250 (Bio-Rad). Western blotting and quantitative mass spectrometry analyses also confirmed the presence of proteins.

DNA substrates

For the DNA binding affinity studies, DNA duplex R5 was prepared by annealing a fluorescently labeled oligonucleotide (Alexa Fluor 488) with the sequence 5′-GTTAGGGTTAGGGTTAGGGTTAGGGTTAGGGT-TAG-3′ and its complementary strand. The sequence of R5 was designed in accordance with the optimal binding site of TRF2 defined by the de Lange laboratory [52]. The substrate was purified using a Mono Q 5/50 GL column (GE Healthcare) with a gradient of 50–1000 mM LiCl in 25 mM Tris–HCl (pH 7.5). All oligonucleotides were purchased from Sigma-Aldrich.

Fluorescence anisotropy

Measurements of TRF1–TIN2 and TRF2–TIN2 binding to telomeric DNA duplex R5 labeled by Alexa Fluor 488 were performed on a FluoroMax-4 spectrofluorometer (Horiba Jobin Yvon, Edison, NJ). Fluorescence anisotropy was monitored at an excitation wavelength of 490 nm and emission wavelength of 520 nm. The slit width (both excitation and emission) for all measurements was 9 nm and the integration time was 1 s. The cuvette contained 1.4 ml of DNA duplex R5 (7.5 nM) in a buffer containing 50 mM sodium phosphate (pH 7.0) and 50 mM NaCl. The protein mixture was titrated into the DNA solution in the cuvette and measured after a 2-min incubation at 25 °C. Fluorescence anisotropy at each titration step was measured five times and averaged with relative standard deviation always lower than 3%. The values of dissociation constants were determined by non-linear least square fits according to the equation $r = r^{MAX}c/(K_D + c)$ using ORIGIN® 2018 (OriginLab, Northampton, MA) and confirmed by symbolic equation-based fitting using Dynafit [53].

Fluorescent protein labeling

Fluorescent protein labeling was performed according to the protocol provided by the supplier with the following modifications. Alexa Fluor 488, carboxylic acid, 2,3,5,6-tetrafluorophenyl ester or Alexa Fluor 594 carboxylic acid, succinimidyl ester (Molecular Probes–Invitrogen) in 4-fold molar excess over protein were diluted in 1/10 protein volume of 1 M sodium bicarbonate, fluorophores were mixed with protein (1 mg) and incubated for 1 h at 4 °C while stirring. The mixture was loaded on PD-10 columns (GE Healthcare) and eluted with 50 mM sodium phosphate (pH 7.0) and 50 mM NaCl. The degrees of labeling—dye/protein ratio—were 95% for TRF1, 93% for TRF2 and 97% for TIN2, as determined by UV/Vis spectroscopy.

Theoretical concept of FCS and FCCS

Fluorescence correlation spectroscopy (FCS) describes spontaneous fluorescence intensity fluctuations caused by rapidly diffusing molecules in a microscopic detection volume (about one femtoliter). FCS determines mobility and kinetics at single-molecule precision [39]. FCCS monitors two different fluorescence signals (two colors) collected at the same time and determines how their coincident fluctuations correlate to each other if the proteins are moving together. FCCS describes binding of measured proteins independently of diffusion rate. The cross-correlation function of two-color system, with one green-labeled particle G and the second with red-labeled particle R, is described as follows

$$G_{GR}(\tau) = \frac{\langle \delta F_G(t) \cdot \delta F_R(t + \tau) \rangle}{\langle F_G(t) \cdot F_R(t) \rangle} \qquad (1)$$

where $F_G(t)$ and $F_R(t)$ correspond to fluorescence intensity fluctuations of individual signals (green and red) and τ represents lag time—the time period that

two proteins stay in confocal volume together. A typical cross-correlation curve is a sigmoidal curve with the highest amplitude in time $t(0)$. With longer lag time, the amplitude decreases, as the probability that two proteins are bound and stay in the confocal volume is lower with increasing time. The single-molecule nature of FCCS measurements causes that relative cross-correlation amplitudes of the same sample fluctuate within standard error, because different number of molecules is detected in confocal volume at different times. The cross-correlation fit with an appropriate model provides us with the degree of complexation of two fluorescently labeled molecules. Under ideal conditions (absence of fluorescence resonance energy transfer and spectral crosstalk of used fluorophores), the cross-correlation amplitude $G_{GR}(0)$ is directly proportional to the concentration of bound species [39,41].

Relative cross-correlation as a measure of binding

In FCCS experiments, we used TIN2 labeled with Alexa Fluor 488 and TRF1 or TRF2 labeled with Alexa Fluor 594, if not stated otherwise. For data evaluation, we refer to relative cross-correlation calculated as a ratio between amplitude of cross-correlation function $G_{TIN2-TRF}(0)$ and auto-correlation function $G_{TIN2}(0)$. In other words, the relative cross-correlation corresponds to the proportion of cross-correlation amplitude related to the TIN2 auto-correlation amplitude. This approach also allowed us to normalize the data regarding their concentration so we could directly compare the results of all measured FCCS experiments [39].

Conditions for microscopy imaging and spectroscopy measurements

All the FCCS measurements were performed with a confocal laser scanning microscope Zeiss LSM 780 using dedicated software ZEN Studio with additional FCS module. For excitation, the Ar^+ laser was used with 488- and 561-nm continuous wave. The emission filters were tuned to minimize crosstalk between Alexa Fluor 488 and Alexa Fluor 594 [54]. To determine the crosstalk, we carried out a FCCS measurement of a mixture of free fluorophores Alexa Fluor 488 and Alexa Fluor 594 that served also as a negative control with minimal cross-correlation (Supplementary Fig. S1). To determine the maximal cross-correlation, we used DNA duplex with two fluorophores attached to opposite ends as a positive control. The positive control consisted of Cy5 and Alexa Fluor 488-labeled 40-mer oligonucleotide with the sequence 5′-[Cy5]-TACTAGTT-CACCGTCAGATCCACTAGCACGCTAG-TTCGAT-[Alexa488]-3′ that was hybridized with its complementary strand. The positive control was

measured under the same conditions as the negative control. Confocal pinhole was fixed to 1 AU, and it was additionally fine adjusted in x, y directions prior to FCCS measurement to maximize the count rate of fluorescence fluctuations. We used "FCS approved" water immersion objective (Zeiss 63x C-Apochromat NA 1.2 W Corr), which guarantees overlap of the point spread function for different wavelengths and correction for any spherical aberration.

Fluorescently labeled TIN2 and TRF1 or TRF2 were incubated at 25 °C at 1 μM concentration to form a complex. The sample was diluted to the final concentration that guaranteed the optimal amount of labeled proteins diffusing through the confocal volume at the same time (up to five proteins) corresponding to concentration 10–20 nM.

Prepared samples were incubated at room temperature, diluted with 50 mM sodium phosphate buffer (pH 7.0) with 50 mM NaCl to a final volume of 200 μl and loaded into a μ-slide 8-well Glass Bottom Chamber (Ibidi). The sample covered the entire bottom of the well. Measurements were started immediately, without further incubation.

For each experiment, raw data containing 50 repetitions of 10-s acquisition were collected and averaged. This approach ensured that we collected enough data to obtain statistically significant values. The raw data were exported and analyzed with software QuickFit 3 [55]. Correlation curves were averaged and fitted with two-component 3D Normal Diffusion model by solving the Levenberg–Marquardt nonlinear least-squares fitting routine. The data were visualized by ORIGIN® 2018 (OriginLab, Northampton, MA). The experiments were performed in triplicate. *P*-values were calculated using two-tailed Student's *t* test by Statistica 13 (Dell).

Size-exclusion chromatography

Protein samples for size-exclusion chromatography were centrifuged and filtered through 0.22-μm membrane filters to avoid aggregations. TRF1, TIN2, TPP1 and TRF2 were mixed and incubated in the same order as they appear. The protein molar ratios were preserved in accordance with the FCCS measurements (TRF1/TRF2/TIN2/TPP1 2:2:1:1). TRF1 and TRF2 were labeled by Alexa Fluor 594 and Alexa Fluor 488, respectively. Superdex™ 10/300 GL column with 50 mM NaCl and 50 mM phosphate (pH 7.0) as mobile phase and flow rate 0.5 ml/min was used for the chromatographic separation. Fractions corresponding to the numbered peaks were collected and analyzed on SDS-PAGE. Labeled proteins in gels were detected using Typhoon™ FLA 9500 detection system. Collected fractions were characterized by Dynamic Light Scattering (Fig. S9) to verify TRF1–TIN2–TRF2–TPP1 complex formation.

Acknowledgments

Appendix A. Supplementary data

Supplementary data to this article can be found online at https://doi.org/10.1016/j.jmb.2019.05.038.

References

[1] E.H. Blackburn, Switching and signaling at the telomere, Cell. 106 (2001) 661–673.

[2] C.W. Greider, E.H. Blackburn, Identification of a specific telomere terminal transferase activity in tetrahymena extracts, Cell. 43 (1985) 405–413.

[3] I. Schmutz, T. de Lange, Shelterin, Curr. Biol. 26 (2016) R397-R9.

[4] T. de Lange, Shelterin: the protein complex that shapes and safeguards human telomeres, Genes Dev. 19 (2005) 2100–2110.

[5] J. Nandakumar, T.R. Cech, Finding the end: recruitment of telomerase to telomeres, Nat Rev Mol Cell Biol. 14 (2013) 69–82.

[6] T. Bilaud, C.E. Koering, E. BinetBrasselet, K. Ancelin, A. Pollice, S.M. Gasser, et al., The telobox, a Myb-related telomeric DNA binding motif found in proteins from yeast, plants and human, Nucleic Acids Res. 24 (1996) 1294–1303.

[7] Z. Zhong, L. Shiue, S. Kaplan, T. de Lange, A mammalian factor that binds telomeric TTAGGG repeats in vitro, Mol. Cell. Biol. 12 (1992) 4834–4843.

[8] J.D. Griffith, L. Comeau, S. Rosenfield, R.M. Stansel, A. Bianchi, H. Moss, et al., Mammalian telomeres end in a large duplex loop, Cell. 97 (1999) 503–514.

[9] Y. Doksani, J.Y. Wu, T. de Lange, X. Zhuang, Super-resolution imaging of telomeres reveals TRF2-dependent T-loop formation, Cell. 155 (2013) 345–356.

[10] D. Van Ly, R.R.J. Low, S. Frölich, T.K. Bartolec, G.R. Kafer, H.A. Pickett, et al., Telomere loop dynamics in chromosome end protection, Mol. Cell 71 (2018) 510–525 (e6).

[11] I. Necasova, E. Janouskova, T. Klumpler, C. Hofr, Basic domain of telomere guardian TRF2 reduces D-loop unwinding whereas Rap1 restores it, Nucleic Acids Res. 45 (2017) 12170–12180.

[12] E. Janouskova, I. Necasova, J. Pavlouskova, M. Zimmermann, M. Hluchy, V. Marini, et al., Human Rap1 modulates TRF2 attraction to telomeric DNA, Nucleic Acids Res. 43 (2015) 2691–2700.

[13] J.Z.S. Ye, J.R. Donigian, M. van Overbeek, D. Loayza, Y. Luo, A.N. Krutchinsky, et al., TIN2 binds TRF1 and TRF2 simultaneously and stabilizes the TRF2 complex on telomeres, J. Biol. Chem. 279 (2004) 47264–47271.

[14] B.R. Houghtaling, L. Cuttonaro, W. Chang, S. Smith, A dynamic molecular link between the telomere length regulator TRF1 and the chromosome end protector TRF2, Curr. Biol. 14 (2004) 1621–1631.

[15] D. Liu, A. Safari, M.S. O'Connor, D.W. Chan, A. Laegeler, J. Qin, et al., PTOP interacts with POT1 and regulates its localization to telomeres, Nat. Cell Biol. 6 (2004) 673.

[16] J.Z.S. Ye, D. Hockemeyer, A.N. Krutchinsky, D. Loayza, S.M. Hooper, B.T. Chait, et al., POT1-interacting protein PIP1: a telomere length regulator that recruits POT1 to the TIN2/TRF1 complex, Genes Dev. 18 (2004) 1649–1654.

[17] P. Baumann, T.R. Cech, Pot1, the putative telomere end-binding protein in fission yeast and humans, Science. 292 (2001) 1171–1175.

[18] Y. Chen, Y. Yang, M. van Overbeek, J. Donigian, P. Baciu, T. de Lange, et al., A shared docking motif in TRF1 and TRF2 used for differential recruitment of telomeric proteins, Science. 319 (2008) 1092–1096.

[19] C. Hu, R. Rai, C. Huang, C. Broton, J. Long, Y. Xu, et al., Structural and functional analyses of the mammalian TIN2–TPP1–TRF2 telomeric complex, Cell Res. 27 (2017) 1485–1502.

[20] T. de Lange, Shelterin-mediated telomere protection, Annu. Rev. Genet. 52 (52) (2018) 223–247.

[21] Z.X. Zeng, W. Wang, Y.T. Yang, Y. Chen, X.M. Yang, J.A. Diehl, et al., Structural basis of selective ubiquitination of TRF1 by SCFFbx4, Dev. Cell 18 (2010) 214–225.

[22] J.Z.S. Ye, T. de Lange, TIN2 is a tankyrase 1 PARP modulator in the TRF1 telomere length control complex, Nat. Genet. 36 (2004) 618–623.

[23] D. Frescas, T. de Lange, TRF2-tethered TIN2 can mediate telomere protection by TPP1/POT1, Mol. Cell. Biol. 34 (2014) 1349–1362.

[24] T. Kibe, M. Zimmermann, T. de Lange, TPP1 blocks an ATR-mediated resection mechanism at telomeres, Mol. Cell 61 (2016) 236–246.

[25] K.K. Takai, T. Kibe, J.R. Donigian, D. Frescas, T. de Lange, Telomere protection by TPP1/POT1 requires tethering to TIN2, Mol. Cell 44 (2011) 647–659.

[26] S. Kim, C. Beausejour, A.R. Davalos, P. Kaminker, S.J. Heo, J. Campisi, TIN2 mediates functions of TRF2 at human telomeres, J. Biol. Chem. 279 (2004) 43799–43804.

[27] W. Palm, T. de Lange, How shelterin protects mammalian telomeres, Annu. Rev. Genet. 42 (2008) 301–334.

[28] J. Nandakumar, C.F. Bell, I. Weidenfeld, A.J. Zaug, L.A. Leinwand, T.R. Cech, The TEL patch of telomere protein TPP1 mediates telomerase recruitment and processivity, Nature. 492 (2012) 285–291.

[29] A.B. Dalby, C. Hofr, T.R. Cech, Contributions of the TEL-patch amino acid cluster on TPP1 to telomeric DNA synthesis by human telomerase, J. Mol. Biol. 427 (2015) 1291–1303.

[30] F. Wang, E.R. Podell, A.J. Zaug, Y.T. Yang, P. Baciu, T.R. Cech, et al., The POT1-TPP1 telomere complex is a telomerase processivity factor, Nature. 445 (2007) 506–510.

[31] N.D. Nelson, L.M. Dodson, L. Escudero, A.T. Sukumar, C.L. Williams, I. Mihalek, et al., The C-terminal extension unique to the Long isoform of the shelterin component TIN2 enhances its interaction with TRF2 in a phosphorylation- and dyskeratosis congenita cluster-dependent fashion, Mol. Cell. Biol. 38 (2018) e00025-18.

[32] S.A. Savage, N. Giri, G.M. Baerlocher, N. Orr, P.M. Lansdorp, B.P. Alter, TINF2, a component of the shelterin telomere protection complex, is mutated in dyskeratosis congenita, Am. J. Hum. Genet. 82 (2008) 501–509.

[33] G. Sarek, P. Marzec, P. Margalef, S.J. Boulton, Molecular basis of telomere dysfunction in human genetic diseases, Nature Structural &Amp; Molecular Biology. 22 (2015) 867.

[34] K.K. Takai, S. Hooper, S. Blackwood, R. Gandhi, T. de Lange, In vivo stoichiometry of shelterin components, J. Biol. Chem. 285 (2010) 1457–1467.

[35] C.J. Lim, A.J. Zaug, H.J. Kim, T.R. Cech, Reconstitution of human shelterin complexes reveals unexpected stoichiometry and dual pathways to enhance telomerase processivity, Nat. Commun. 8 (2017) 1075.

[36] J. Fan, M. Leroux-Coyau, N.J.S. Avery, T.R. Strick, Reconstruction of bacterial transcription-coupled repair at single-molecule resolution, Nature. 536 (2016) 234–237.

[37] E.T. Graves, C. Duboc, J. Fan, F. Stransky, M. Leroux-Coyau, T.R. Strick, A dynamic DNA-repair complex observed by correlative single-molecule nanomanipulation and fluorescence, Nat. Struct. Mol. Biol. 22 (2015) 452–457.

[38] J.W. Parks, M.D. Stone, Single-molecule studies of telomeres and telomerase, Annu. Rev. Biophys. 46 (2017) 357–377.

[39] K. Bacia, P. Schwille, Practical guidelines for dual-color fluorescence cross-correlation spectroscopy, Nat. Protoc. 2 (2007) 2842.

[40] Hink MA, de Vries SC, Visser AJ. Fluorescence fluctuation analysis of receptor kinase dimerization. Methods Mol. Biol. 2011;779:199–215.

[41] S.A. Kim, K.G. Heinze, M.N. Waxham, P. Schwille, Intracellular calmodulin availability accessed with two-photon cross-correlation, Proc. Natl. Acad. Sci. U. S. A. 101 (2004) 105–110.

[42] M.S. O'Connor, A. Safari, H.W. Xin, D. Liu, Z. Songyang, A critical role for TPP1 and TIN2 interaction in high-order telomeric complex assembly, Proc. Natl. Acad. Sci. U. S. A. 103 (2006) 11874–11879.

[43] D. Liu, M.S. O'Connor, J. Qin, Z. Songyang, Telosome, a mammalian telomere-associated complex formed by multiple telomeric proteins, J. Biol. Chem. 279 (2004) 51338–51342.

[44] S. Grill, V.M. Tesmer, J. Nandakumar, The N terminus of the OB domain of telomere protein TPP1 is critical for telomerase action, Cell Rep. 22 (2018) 1132–1140.

[45] P.L. Privalov, G.I. Makhatadze, Contribution of hydration to protein-folding thermodynamics. 2. The entropy and Gibbs energy of hydration, J. Mol. Biol. 232 (1993) 660–679.

[46] D. Broccoli, A. Smogorzewska, L. Chong, T. de Lange, Human telomeres contain two distinct Myb-related proteins, TRF1 and TRF2, Nat. Genet. 17 (1997) 231–235.

[47] L. Fairall, L. Chapman, H. Moss, T. de Lange, D. Rhodes, Structure of the TRFH dimerization domain of the human telomeric proteins TRF1 and TRF2, Mol. Cell 8 (2001) 351–361.

[48] J.-K. Kim, J. Liu, X. Hu, C. Yu, K. Roskamp, B. Sankaran, et al., Structural basis for shelterin bridge assembly, Mol. Cell 68 (2017) 698–714 (e5).

[49] Armbruster BN, Etheridge KT, Broccoli D, Counter CM. Putative telomere-recruiting domain in the catalytic subunit of human telomerase. 2003;23:3237–3246.

[50] J.G. Lin, P. Countryman, N. Buncher, P. Kaur, E. Longjiang, Y.Y. Zhang, et al., TRF1 and TRF2 use different mechanisms to find telomeric DNA but share a novel mechanism to search for protein partners at telomeres, Nucleic Acids Res. 42 (2014) 2493–2504.

[51] P. Veverka, T. Janovič, C. Hofr, Quantitative biology of human shelterin and telomerase—searching for the weakest point, Int. J. Mol. Sci. (2019) (in revision).

[52] A. Smogorzewska, B. Van Steensel, A. Bianchi, S. Oelmann, M.R. Schaefer, G. Schnapp, et al., Control of human telomere length by TRF1 and TRF2, Mol. Cell. Biol. 20 (2000) 1659–1668.

[53] P. Kuzmic, Program DYNAFIT for the analysis of enzyme kinetic data: application to HIV proteinase, Anal. Biochem. 237 (1996) 260–273.

[54] K. Bacia, Z. Petrasek, P. Schwille, Correcting for spectral cross-talk in dual-color fluorescence cross-correlation spectroscopy, Chemphyschem. 13 (2012) 1221–1231.

[55] J.W. Krieger, A.P. Singh, C.S. Garbe, T. Wohland, J. Langowski, Dual-color fluorescence cross-correlation spectroscopy on a single plane illumination microscope (SPIM-FCCS), Opt. Express 22 (2014) 2358–2375.